

Cite this: *Mater. Adv.*, 2022,  
3, 2185Received 10th November 2021,  
Accepted 9th January 2022

DOI: 10.1039/d1ma01050f

rsc.li/materials-advances

## Preparation of heterostructured TiO<sub>2</sub>/MoS<sub>2</sub> for efficient photocatalytic rhodamine B degradation†

Ping Li,<sup>‡a</sup> Mengyou Gao,<sup>‡ab</sup> Lei Sun,<sup>a</sup> Huizhong Xu,<sup>a</sup> Xiaochen Dong<sup>id</sup><sup>c</sup> and Jianjian Lin<sup>id</sup><sup>\*a</sup>

Coating a few layers of MoS<sub>2</sub> nanosheets on a substrate is an effective approach to enhance catalytic activity for photocatalytic degradation. Herein, we fabricated heterostructured TiO<sub>2</sub>/MoS<sub>2</sub> (H-TiO<sub>2</sub>/MoS<sub>2</sub>) with high structural stability via a simple two-step solvothermal approach. H-TiO<sub>2</sub>/MoS<sub>2</sub> was composed of TiO<sub>2</sub> as a hard core and MoS<sub>2</sub> nanosheets as a shell, which could increase the electron transfer rate between TiO<sub>2</sub> and MoS<sub>2</sub> and enable active edge sites of MoS<sub>2</sub> to be maximally exposed. Besides, H-TiO<sub>2</sub>/MoS<sub>2</sub> indicated enhanced light absorption in the UV to Vis range when compared to TiO<sub>2</sub> nanoparticles, and slightly lower than that of MoS<sub>2</sub>. This is beneficial for the enhancement of the photocatalytic degradation performance. Therefore, H-TiO<sub>2</sub>/MoS<sub>2</sub> displayed a strong adsorption ability toward organic dyes and showed excellent performance in the photocatalytic degradation of rhodamine B with the concentration decreased by 99.4% due to the synergistically stimulative effect. The work will enlighten the development of highly efficient molybdenum sulfide-based heterostructured photocatalysts.

## Introduction

Nowadays, semiconductor photocatalysts are attracting increasing attention owing to their high efficiency in easing the energy crisis and reducing environmental pollution. Recently, a large variety of semiconductor photocatalysts have been explored including TiO<sub>2</sub>,<sup>1,2</sup> SrTiO<sub>3</sub>,<sup>3</sup> *etc.*, which were mainly active in the ultraviolet range, and C<sub>3</sub>N<sub>4</sub>,<sup>4</sup> Cu<sub>2</sub>O, Co<sub>3</sub>O<sub>4</sub>,<sup>5</sup> CdS,<sup>6</sup> *etc.* that have high visible light activity. TiO<sub>2</sub>, as an n-type photocatalytic semiconductor, is efficient for the separation of electrons and holes. Furthermore, it has both good chemical and physical stability, relatively low cost and nontoxicity, and thus has a wide range of applications in various fields, such as self-cleaning and removal of hazardous compounds. However, the large band gap of TiO<sub>2</sub> (3.2 eV) has become the main drawback because limited UV light could be used, which significantly decreased the photocatalytic performance. Additionally, pure TiO<sub>2</sub> usually did not have a high charge separation rate, and therefore illustrated relatively low

photocatalytic activity. Thus, many research studies have been conducted to settle these inadequacies including tuning the particle size,<sup>7</sup> crystallinity and morphologies (nanotubes<sup>8</sup> in 1D, nanosheets<sup>9</sup> in 2D and microspheres<sup>10</sup> or nanoflowers<sup>11</sup> in 3D), and constructing heterostructured materials,<sup>12–14</sup> which have resulted in the promotion of the photocatalytic performance. Among these nanostructures, heterostructures like core-shell structures<sup>15</sup> with a large specific surface area and matched energy levels have attracted great attention.

Moreover, it has been reported that TiO<sub>2</sub>-based photocatalysts doped with cocatalysts like noble metals,<sup>10</sup> MoS<sub>2</sub>,<sup>16–18</sup> *etc.*, could broaden the range of light harvesting from the UV to UV-vis, and improve the charge separation efficiency. Two-dimensional transition metal sulfides (2D MS<sub>x</sub>), such as the typical MoS<sub>2</sub>, were reported as platinum-like materials, which were beneficial for improving the photocatalytic performance as a cocatalyst because of great (photo) electronic and catalytic traits.<sup>19</sup> In addition, a few-layered MoS<sub>2</sub> with increased edges was beneficial for electron acceptance, as well as increased active sites, illustrating improved photocatalytic performance. Recently, MoS<sub>2</sub> catalysts with a variety of nanostructures have been prepared using various approaches including chemical vapour deposition,<sup>20</sup> thermolysis<sup>21</sup> or hydrothermal and solvothermal methods.<sup>22</sup> Irregular aggregates of nanoparticles or stacked multilayers of the as-fabricated MoS<sub>2</sub>, however, largely limited the photocatalytic performance. Therefore, preparing heterostructured MoS<sub>2</sub>-based photocatalysts with enhanced photocatalytic activity remains challenging. Recently, MoS<sub>2</sub>-based photocatalysts such as CdS/MoS<sub>2</sub>,<sup>23,24</sup> graphene/

<sup>a</sup> Shandong Key Laboratory of Biochemical Analysis, College of Chemistry and Molecular Engineering, Qingdao University of Science and Technology, Qingdao 266042, P. R. China. E-mail: Jianjian\_Lin@qust.edu.cn

<sup>b</sup> College of Automation and Electronic Engineering, Qingdao University of Science and Technology, Qingdao 266042, P. R. China

<sup>c</sup> Key Laboratory of Flexible Electronics (KLOFE) & Institute of Advanced Materials (IAM), Nanjing Tech University (NanjingTech), 30 South Puzhu Road, Nanjing, 211800, P. R. China

† Electronic supplementary information (ESI) available. See DOI: 10.1039/d1ma01050f

‡ These authors equally contributed to this work



MoS<sub>2</sub><sup>25,26</sup> and TiO<sub>2</sub>/MoS<sub>2</sub> heterostructures with various structures including particles<sup>27</sup> (0D), belts<sup>28</sup> and wires<sup>12</sup> (1D), sheets<sup>29</sup> (2D) and flowers<sup>30</sup> (3D) have demonstrated enhanced photocatalytic activities. Meanwhile, constructing novel nanostructures of core-shelled TiO<sub>2</sub>/MoS<sub>2</sub> is also an effective approach to develop photocatalysts with large specific surface areas and increased active sites.

In this work, we prepared H-TiO<sub>2</sub>/MoS<sub>2</sub> through a two-step solvothermal approach. In the first step, TiO<sub>2</sub> nanoparticles were prepared as an ellipsoidal core through a solvothermal approach; then MoS<sub>2</sub> nanosheets were coated on the surface of the TiO<sub>2</sub> precursor again using a solvothermal method. The MoS<sub>2</sub> nanosheets which were coated on the surface of TiO<sub>2</sub> nanoparticles could allow fast electron transfer between TiO<sub>2</sub> and MoS<sub>2</sub>. Furthermore, H-TiO<sub>2</sub>/MoS<sub>2</sub> illustrated good structural stability. MoS<sub>2</sub> nanosheets could expose active edge sites maximally, allowing an enhanced adsorption ability and improved photocatalytic degradation performance of rhodamine B (RhB). The synergistic effect of the novel heterostructure between MoS<sub>2</sub> nanosheets and TiO<sub>2</sub> nanoparticles accounted for the outstanding photocatalytic degradation performance.

## Experimental

### Chemicals

Tetrabutyl titanate (TBT, Aladdin Biochemical Technology Co., Ltd) and glacial acetic acid (Macklin Co., Ltd) were used without further purification. Absolute ethanol and Na<sub>2</sub>MoO<sub>4</sub>·2H<sub>2</sub>O were purchased from Sinopharm Chemical Regent Co., Ltd. Cysteine was purchased from Beijing Xingjingke Biotechnology Co., Ltd. Ultrapure H<sub>2</sub>O was employed in all experiments.

### Preparation of TiO<sub>2</sub>

In a typical synthesis process, the TiO<sub>2</sub> precursor was synthesized by a hydrothermal strategy.<sup>7,31</sup> In detail, TBT (1 mL) was dropped into glacial acetic acid (15 mL) at room temperature, followed by addition of ultrapure water (0.3 mL) to initiate the hydrolysis of TBT. The mixture was stirred for ~10 minutes at room temperature, and then transferred into a 50 mL autoclave, which was heated at 150 °C for 12 h. The as-prepared precursor was obtained by centrifugation after cooling the autoclave to room temperature and washed thoroughly with absolute ethanol and water several times with the assistance of ultrasound treatment.

### Synthesis of H-TiO<sub>2</sub>/MoS<sub>2</sub>

H-TiO<sub>2</sub>/MoS<sub>2</sub> was prepared *via* a solvothermal method.<sup>22</sup> In detail, 100 mg TiO<sub>2</sub> was dissolved into C<sub>2</sub>H<sub>5</sub>OH (10 mL) and H<sub>2</sub>O (20 mL), then Na<sub>2</sub>MoO<sub>4</sub>·2H<sub>2</sub>O (0.3 g) and cysteine (1.25 g) were added under vigorous stirring in sequence. Then the mixed solution was transferred into an autoclave (50 mL) and heated at 200 °C for 24 h. The resultant sample was obtained by centrifugation after cooling the autoclave to room temperature. Finally, the obtained sample was washed thoroughly with

absolute ethanol and water several times with the assistance of ultrasound treatment. The as-fabricated H-TiO<sub>2</sub>/MoS<sub>2</sub> was heated at 800 °C (5 °C min<sup>-1</sup>) under an Ar (5% H<sub>2</sub>) atmosphere for 2 h before collection.

### Characterization

X-Ray diffraction (Bruker D8 Advance) with Ni-filtered Cu K $\alpha$  radiation was used to reveal the crystal structure of the as-prepared samples at 40 kV and 40 mA with a step size of 0.02° and scan speed of 0.1 s. Transmission electron microscopy (TEM, FEI Tecnai G2 F20) and scanning electron microscopy (SEM, Zeiss Merlin compact LE0 1530 VP) were used to explore the morphologies and elemental compositions of the as-prepared samples. The Raman spectrum of TiO<sub>2</sub>/MoS<sub>2</sub> was recorded on an Invia Qontor. Fourier transform-infrared (FT-IR) spectroscopy was performed to confirm the spectrum of TiO<sub>2</sub>/MoS<sub>2</sub> in the range of 400–4000 cm<sup>-1</sup> using a PerkinElmer Spectrum One spectrometer. N<sub>2</sub> adsorption and desorption curves were obtained for the analysis of pore structure by ASAP 2460. UV-Vis absorption spectra were recorded on a PerkinElmer (Lambda 1050 +) for revealing the light absorption of the as-prepared samples.

### Photocatalytic degradation measurement

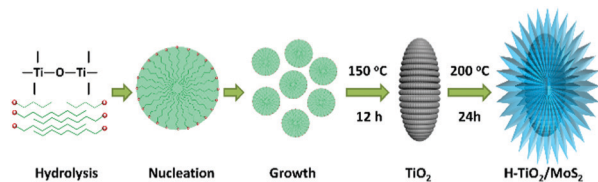
Photocatalytic activity was studied at room temperature by the degradation of RhB using a 300 W Xe lamp. For the photocatalytic test, 50 mL of an aqueous suspension of RhB (15 mg L<sup>-1</sup>) and 5 mg of the samples were placed in a Pyrex glass tube. Before irradiation, the suspension was sonicated and stirred for 30 min in the dark. The mixed solution was continuously stirred during the photocatalytic reaction. During the photocatalytic reaction process, 3 mL of the suspension were collected after irradiation for the following analysis after the filtration. The concentration of RhB was monitored by measuring the absorbance at 554 nm using a UV-vis spectrometer (Lambda 1050 +). Isopropanol, DMSO and *t*-BuOH were used as free radical scavengers for the scavenging experiments. The pH values of RhB solution were controlled by 0.1 M HCl and 0.1 M NaOH.

## Results and discussion

### Morphology and composition

As illustrated in Scheme 1, H-TiO<sub>2</sub>/MoS<sub>2</sub> was fabricated *via* a simple two-step method. Initially, the porous TiO<sub>2</sub> (rice-like) precursor was prepared *via* a facile solvothermal method;<sup>7,31</sup> then the TiO<sub>2</sub> precursor was seen as a hard core, which loaded MoS<sub>2</sub> as a shell outside, resulting in the successful preparation of H-TiO<sub>2</sub>/MoS<sub>2</sub>. Firstly, the tetrabutyl titanate precursor was hydrolyzed and nucleated into TiO<sub>2</sub> microcrystals, and then the microcrystals gradually grew as porous TiO<sub>2</sub>. In detail, the tetrabutyl titanate precursor was hydrolyzed into numerous winding chain bundles after 2 h of reaction (Fig. S1a, ESI†). As the reaction proceeds, some chain bundles are gradually rotated and twisted into ellipsoidal aggregates which can serve as crystal nuclei.<sup>31</sup> Finally, after 12 h of reaction, all the





Scheme 1 Scheme of the preparation process for as-prepared H-TiO<sub>2</sub>/MoS<sub>2</sub>.

ellipsoidal aggregates grew into ellipsoidal particles (Fig. S1b, ESI<sup>†</sup>). The H-TiO<sub>2</sub>/MoS<sub>2</sub> heterostructure was formed by an L-cysteine-assisted method.<sup>22,32</sup> For the self-assembly process of the H-TiO<sub>2</sub>/MoS<sub>2</sub> heterostructure, the porous TiO<sub>2</sub> served as a precursor core for the adsorption of MoO<sub>4</sub><sup>2-</sup> anions. When heated in the solution-phase reaction, L-cysteine can release H<sub>2</sub>S, meanwhile acting as a sulfide source and a reducing agent.<sup>32</sup> As the reaction time increased, H<sub>2</sub>S *in situ* reacted with MoO<sub>4</sub><sup>2-</sup> anions to form a two-dimensional nano-plate-like structure, which is common in other MoS<sub>2</sub>-based composites.<sup>33–35</sup> As illustrated in Fig. S2 (ESI<sup>†</sup>), MoS<sub>2</sub> can be loaded onto the surface of TiO<sub>2</sub> in a short time and gradually crystallize with time.

As shown in X-ray diffraction patterns of Fig. 1, the crystal structure of the as-prepared precursor can be confirmed as TiO<sub>2</sub> (anatase, Fig. S3a, ESI<sup>†</sup> JCPDS No. 21-1272).<sup>7,31</sup> Besides, the crystal structure of the resultant sample was confirmed to be H-TiO<sub>2</sub>/MoS<sub>2</sub>, which corresponds to TiO<sub>2</sub> and MoS<sub>2</sub> (2H, Fig. S3b, ESI<sup>†</sup> JCPDS No. 37-1492)<sup>22</sup> phases, indicating that H-TiO<sub>2</sub>/MoS<sub>2</sub> was fabricated successfully.

To indicate the porous structure of TiO<sub>2</sub>, the characterization studies including magnified SEM and TEM images and N<sub>2</sub> adsorption and desorption curves of a single TiO<sub>2</sub> particle were performed. As illustrated in Fig. S4a and b (ESI<sup>†</sup>), the SEM and TEM images showed that the TiO<sub>2</sub> particle had plenty of pores, and the N<sub>2</sub> adsorption and desorption curves demonstrated a specific surface area of 103.07 m<sup>2</sup> g<sup>-1</sup> for TiO<sub>2</sub> particles (Fig. S4c, ESI<sup>†</sup>).

The morphology of H-TiO<sub>2</sub>/MoS<sub>2</sub> (~240 nm) was confirmed by SEM and TEM. The SEM image in Fig. 2a illustrated that MoS<sub>2</sub> nanosheets (~20 nm thickness) were coated on the surface of TiO<sub>2</sub> nanoparticles successfully, which matched well

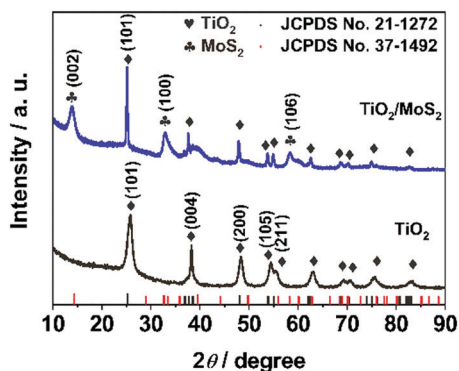


Fig. 1 XRD patterns of as-prepared TiO<sub>2</sub> and H-TiO<sub>2</sub>/MoS<sub>2</sub>.

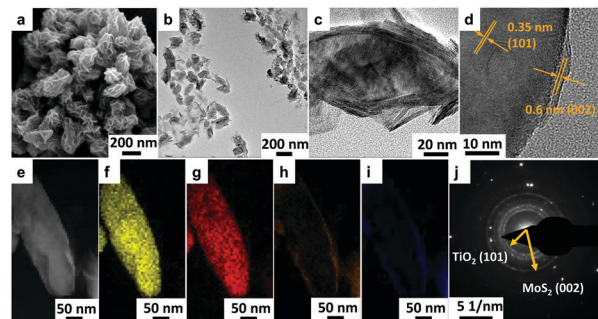


Fig. 2 (a) SEM, (b) low- and (c) high-magnification TEM image, (d) HRTEM image, (e–i) STEM EDS mapping images and (j) SAED image of H-TiO<sub>2</sub>/MoS<sub>2</sub>.

with the TEM image in Fig. 2b. Additionally, the single magnified particle in Fig. 2c clearly showed that a few layer MoS<sub>2</sub> (~10–30 layers) was loaded onto the surface of TiO<sub>2</sub>. What is more, as illustrated in the high-resolution TEM (HRTEM) image of Fig. 2d, the lattice fringe of 0.35 nm corresponded to the (101) plane of TiO<sub>2</sub>, and a lattice fringe of 0.6 nm corresponded to the (002) facet of MoS<sub>2</sub>.<sup>36</sup> In order to explore the element dispersion of H-TiO<sub>2</sub>/MoS<sub>2</sub>, scanning transmission electron microscopy energy dispersive spectroscopy (STEM EDS) was employed. As shown in Fig. 2e–i, Ti and O were distributed evenly inside as a core, while Mo and S were located outside as a shell, demonstrating that MoS<sub>2</sub> encapsulated on the surface of TiO<sub>2</sub> successfully, which was consistent with SEM and TEM results.

Furthermore, the selected area electron diffraction (SAED) pattern in Fig. 2j pointed to the TiO<sub>2</sub> (101) facet and MoS<sub>2</sub> (002) facet, and corresponds well with the HRTEM image in Fig. 2d.

The rice-like morphology of the as-fabricated TiO<sub>2</sub> is clearly shown in Fig. 3a with ~200 nm in length and ~70 nm in width. Meanwhile, MoS<sub>2</sub> flowers were prepared and are shown in the SEM image in Fig. 3b.

The Raman scattering spectrum in Fig. 4a illustrated a series of Raman peaks of the as-prepared H-TiO<sub>2</sub>/MoS<sub>2</sub>, which corresponded to the typical peaks of MoS<sub>2</sub> and TiO<sub>2</sub>. The peak located at 379 cm<sup>-1</sup> was attributed to the in-plane E<sub>2g</sub> mode, while the peak located at 404 cm<sup>-1</sup> was ascribed to the out-of-plane A<sub>1g</sub> mode of MoS<sub>2</sub>.<sup>37</sup> Meanwhile, the Raman peak located at 144 cm<sup>-1</sup> corresponded to the E<sub>1g</sub> mode of TiO<sub>2</sub>. The FT-IR spectrum of the as-prepared H-TiO<sub>2</sub>/MoS<sub>2</sub> is shown in Fig. 4b. There are broad bands of H-TiO<sub>2</sub>/MoS<sub>2</sub> at 486 cm<sup>-1</sup>, 903 cm<sup>-1</sup>, 1122 cm<sup>-1</sup>, and 1640 cm<sup>-1</sup>.<sup>38</sup> The band which was located at

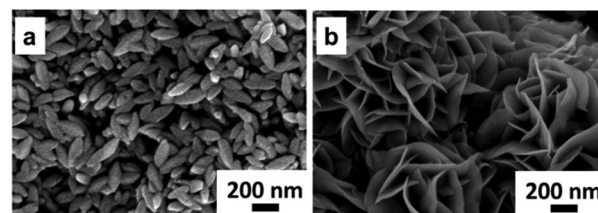


Fig. 3 SEM images of (a) TiO<sub>2</sub> nanoparticles and (b) MoS<sub>2</sub> flowers.



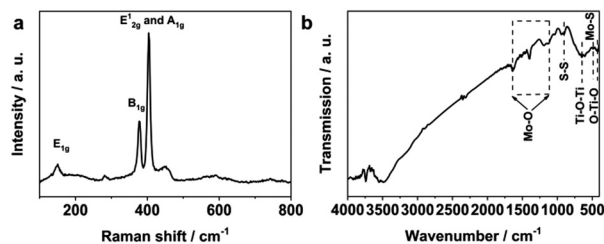


Fig. 4 Raman and FTIR spectra of as-prepared H-TiO<sub>2</sub>/MoS<sub>2</sub>.

486 cm<sup>-1</sup> corresponded to the Mo-S bond, while the band situated at 903 cm<sup>-1</sup> was assigned to the S-S bond. The bands between 1122 cm<sup>-1</sup> and 1640 cm<sup>-1</sup> were ascribed to the stretching vibrations of -OH and Mo-O.

### Photo absorption and photocatalytic degradation of RhB

UV-Vis absorption spectra were obtained to understand the optical properties. As illustrated in Fig. S5 (ESI<sup>†</sup>), H-TiO<sub>2</sub>/MoS<sub>2</sub> showed enhanced light absorption in the UV to Vis range when compared to TiO<sub>2</sub> nanoparticles, which is slightly lower than that of MoS<sub>2</sub>. The photocatalytic degradation of RhB for H-TiO<sub>2</sub>/MoS<sub>2</sub> was evaluated under a 300 W Xe lamp (Fig. 5a). Before light irradiation, the photocatalyst went through an adsorption process in RhB solution in the dark for 30 min. Interestingly, it is found that H-TiO<sub>2</sub>/MoS<sub>2</sub> illustrated a stronger adsorption ability towards RhB than TiO<sub>2</sub> nanoparticles and MoS<sub>2</sub> flowers, which was reported have an efficient photocatalytic performance. In addition, the RhB photodegradation efficiency of H-TiO<sub>2</sub>/MoS<sub>2</sub> was greater than that of TiO<sub>2</sub> nanoparticles and slightly higher than that of MoS<sub>2</sub> flowers, suggesting the advantages of H-TiO<sub>2</sub>/MoS<sub>2</sub> nanostructures. Specifically, the concentrations of RhB were decreased by 32.6%, 36.2%, and 29.6% after irradiation with catalyst of H-TiO<sub>2</sub>/MoS<sub>2</sub>, TiO<sub>2</sub> nanoparticles, and MoS<sub>2</sub> flowers, respectively. It is remarkable that the concentration of RhB decreased by 99.4% using H-TiO<sub>2</sub>/MoS<sub>2</sub>, which was beneficial for RhB adsorption and degradation. As shown in Fig. 5b, the recycling stability of H-TiO<sub>2</sub>/MoS<sub>2</sub> was tested for 5 cycles, and illustrated no evident decay, which demonstrated a good stability.

Additionally, as illustrated in Fig. S6 (ESI<sup>†</sup>), the consumed time for degradation decreased as the pH value increased. Specifically, it only took 20 min for RhB degradation at pH = 3, while it took ~50 min for RhB degradation at pH = 6.9 and 8.9. This indicated that the degradation of RhB was easier in acid solution.

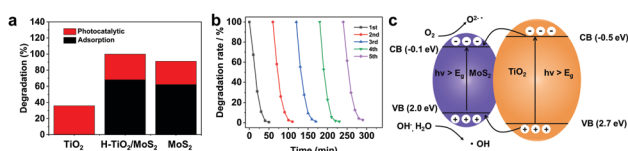


Fig. 5 (a) Adsorption of RhB in dark (30 min) and photocatalytic degradation of RhB under the light irradiation (40 min) with TiO<sub>2</sub> nanoparticles, H-TiO<sub>2</sub>/MoS<sub>2</sub> and MoS<sub>2</sub> flowers. (b) The recycling stability and (c) schematic photocatalytic degradation principle of H-TiO<sub>2</sub>/MoS<sub>2</sub>.

The schematic diagram (Fig. 5c) illustrates the energy band structure of H-TiO<sub>2</sub>/MoS<sub>2</sub> and the process of electron transfer and the formation process of reactive oxygen species. Generally, the band gap of TiO<sub>2</sub> (anatase) was relatively wide (~3.2 eV), while the band gap of MoS<sub>2</sub> was narrower (~1.8 eV).<sup>39</sup> Upon light illumination, electrons could be excited from the valence band (VB) of MoS<sub>2</sub> to the conduction band (CB), leaving holes in the VB. Compared with TiO<sub>2</sub>, it was easy to induce photo-generated electrons in MoS<sub>2</sub> with a relatively lower CB, and the photo-induced electrons (CB, MoS<sub>2</sub>) could rapidly transport to TiO<sub>2</sub> nanoparticles (CB). The Mott-Schottky test was carried out to determine the flat-band potential of H-TiO<sub>2</sub>/MoS<sub>2</sub>.<sup>40</sup> As illustrated in Fig. S7 (ESI<sup>†</sup>), the potential can be confirmed to be ~-0.47 V (vs. SCE). The corresponding potential was converted to 0.18 V (vs. RHE) according to the equation  $E$  (vs. RHE) =  $E$  (vs. SCE) + 0.0591 pH + 0.244 V. Owing to dissolved oxygen in solution, photo-induced electrons could form superoxide radical anions from trapped O<sub>2</sub> (O<sub>2</sub> + e<sup>-</sup> → O<sub>2</sub><sup>•-</sup>), O<sub>2</sub><sup>•-</sup>, as a high activity intermediate, usually used to degrade organic pollutants. On the valence band, the leaving holes were transferred from TiO<sub>2</sub> to MoS<sub>2</sub> due to the higher VB, H<sub>2</sub>O was oxidized into hydroxyl radicals by holes with strong reduction (H<sub>2</sub>O + h<sup>+</sup> → •OH), which could oxidize organic dye into CO<sub>2</sub> and H<sub>2</sub>O, etc.<sup>41</sup> The active species generated in the process of photodegradation were h<sup>+</sup>, radical O<sub>2</sub><sup>•</sup> and radical •OH.<sup>42</sup> In order to reveal the main active species that played the significant role in the photodegradation of RhB, the free radical scavenging experiments were conducted. In detail, free radical scavengers of isopropanol, dimethylsulfoxide (DMSO) and *t*-BuOH were added to the photodegradation system as a h<sup>+</sup> trapping agent, a radical O<sub>2</sub><sup>•-</sup> trapping agent and a radical OH• trapping agent, respectively. As illustrated in Fig. S8 (ESI<sup>†</sup>), the photodegradation efficiency of RhB without adding a trapping agent was 94.7%, and the degradation efficiencies after adding isopropanol, *t*-BuOH and DMSO were 97.0%, 78.5% and 25.4%, respectively. The photodegradation performance of RhB was inhibited notably after adding DMSO, which confirmed that radical O<sub>2</sub><sup>•-</sup> was the main active species used for oxidation and h<sup>+</sup> played a synergistic role in the photocatalytic reaction,<sup>43</sup> and radical •OH indicated no evident effect.<sup>44</sup> H-TiO<sub>2</sub>/MoS<sub>2</sub> was just tapping into its strong charge separation ability and weak charge-hole recombination ability for enhancing the photocatalytic degradation performance.

## Conclusions

H-TiO<sub>2</sub>/MoS<sub>2</sub> consisting of TiO<sub>2</sub> as a hard core and MoS<sub>2</sub> as a shell was prepared through a facile two-step solvothermal approach. H-TiO<sub>2</sub>/MoS<sub>2</sub> was beneficial for fast electron transfer between TiO<sub>2</sub> and MoS<sub>2</sub> due to maximally exposed active edge sites of MoS<sub>2</sub> and illustrated high structural stability. Moreover, H-TiO<sub>2</sub>/MoS<sub>2</sub> indicated enhanced light absorption and improved performance in the photocatalytic degradation of RhB (99.4%). The synergistic effect between MoS<sub>2</sub> nanosheets and TiO<sub>2</sub> nanoparticles accounted for the outstanding photocatalytic



degradation performance. Therefore, this novel photocatalyst is promising for preparing elaborate heterostructures and applications in various fields, such as sewage-treatment, dye degradation, etc.

## Author contributions

Ping Li: data curation, writing – original draft, methodology, investigation. Mengyou Gao: supervision, writing – review and editing. Lei Sun: investigation, data curation. Huizhong Xu: data curation. Xiaochen Dong: methodology, investigation. Jianjian Lin: methodology, conceptualization, supervision, writing – review and editing.

## Conflicts of interest

The authors declare that there are no conflicts to declare.

## Acknowledgements

This work was partly supported by QUSTHX201919. J. Lin is supported by the Young Taishan Scholarship Project of Shandong Province (tsqn201909115).

## Notes and references

- 1 A.-Y. Zhang, W.-Y. Wang, J.-J. Chen, C. Liu, Q.-X. Li, X. Zhang, W.-W. Li, Y. Si and H.-Q. Yu, Epitaxial Facet Junctions on TiO<sub>2</sub> Single Crystals for Efficient Photocatalytic Water Splitting, *Energy Environ. Sci.*, 2018, **11**, 1444–1448.
- 2 W. Zhang, H. He, Y. Tian, K. Lan, Q. Liu, C. Wang, Y. Liu, A. Elzatahry, R. Che, W. Li and D. Zhao, Synthesis of Uniform Ordered Mesoporous TiO<sub>2</sub> Microspheres with Controllable Phase Junctions for Efficient Solar Water Splitting, *Chem. Sci.*, 2019, **10**, 1664–1670.
- 3 L. Mu, Y. Zhao, A. Li, S. Wang, Z. Wang, J. Yang, Y. Wang, T. Liu, R. Chen, J. Zhu, F. Fan, R. Li and C. Li, Enhancing Charge Separation on High Symmetry SrTiO<sub>3</sub> Exposed with Anisotropic Facets for Photocatalytic Water Splitting, *Energy Environ. Sci.*, 2016, **9**, 2463–2469.
- 4 L. Ai, R. Shi, J. Yang, K. Zhang, T. Zhang and S. Lu, Efficient Combination of g-C<sub>3</sub>N<sub>4</sub> and CDs for Enhanced Photocatalytic Performance: A Review of Synthesis, Strategies, and Applications, *Small*, 2021, 2007523.
- 5 L. Wang, J. Wan, Y. Zhao, N. Yang and D. Wang, Hollow Multi-Shelled Structures of Co<sub>3</sub>O<sub>4</sub> Dodecahedron with Unique Crystal Orientation for Enhanced Photocatalytic CO<sub>2</sub> Reduction, *J. Am. Chem. Soc.*, 2019, **141**, 2238–2241.
- 6 R. Shen, D. Ren, Y. Ding, Y. Guan, Y. H. Ng, P. Zhang and X. Li, Nanostructured CdS for Efficient Photocatalytic H<sub>2</sub> Evolution: A Review, *Sci. China Mater.*, 2020, **63**, 2153–2188.
- 7 J. Lin, P. Li, H. Xu, Y. Kim, Z. Jing and D. Zheng, Controlled Synthesis of Mesoporous Single-Crystalline TiO<sub>2</sub> Nanoparticles for Efficient Photocatalytic H<sub>2</sub> Evolution, *J. Hazard. Mater.*, 2020, **391**, 122530.
- 8 P. Petrisková, O. Monfort, L. Satrapinskyy, E. Dobročka, T. Plecenik, G. Plesch, R. Papsík, R. Bermejo and Z. Lenčič, Preparation and Photocatalytic Activity of TiO<sub>2</sub> Nanotube Arrays Prepared on Transparent Spinel Substrate, *Ceram. Int.*, 2021, **47**, 12970–12980.
- 9 X. Tao, P. Ruan, X. Zhang, H. Sun and X. Zhou, Microsphere Assembly of TiO<sub>2</sub> Mesoporous Nanosheets with Highly Exposed (101) Facets and Application in a Light-Trapping Quasi-Solid-State Dye-Sensitized Solar Cell, *Nanoscale*, 2015, **7**, 3539–3547.
- 10 Z. Jiang, W. Wei, D. Mao, C. Chen, Y. Shi, X. Lv and J. Xie, Silver-Loaded Nitrogen-Doped Yolk-Shell Mesoporous TiO<sub>2</sub> Hollow Microspheres with Enhanced Visible Light Photocatalytic Activity, *Nanoscale*, 2015, **7**, 784–797.
- 11 Y. Liu, K. Lan, S. Li, Y. Liu, B. Kong, G. Wang, P. Zhang, R. Wang, H. He, Y. Ling, A. M. Al-Enizi, A. A. Elzatahry, Y. Cao, G. Chen and D. Zhao, Constructing Three-Dimensional Mesoporous Bouquet-Posy-like TiO<sub>2</sub> Superstructures with Radially Oriented Mesochannels and Single-Crystal Walls, *J. Am. Chem. Soc.*, 2017, **139**, 517–526.
- 12 X. Li, W. Li, M. Li, P. Cui, D. Chen, T. Gengenbach, L. Chu, H. Liu and G. Song, Glucose-Assisted Synthesis of the Hierarchical TiO<sub>2</sub> Nanowire@MoS<sub>2</sub> Nanosheet Nanocomposite and Its Synergistic Lithium Storage Performance, *J. Mater. Chem. A*, 2015, **3**, 2762–2769.
- 13 Y. Sun, H. Lin, C. Wang, Q. Wu, X. Wang and M. Yang, Morphology-Controlled Synthesis of TiO<sub>2</sub>/MoS<sub>2</sub> Nanocomposites with Enhanced Visible-Light Photocatalytic Activity, *Inorg. Chem. Front.*, 2018, **5**, 145–152.
- 14 Q. Wang, P. Yu, L. Bai, R. Bao, N. Wang, C. Cheng, Z. Liu, M. Yang, W. Yang and Z. Guo, Self-Assembled Nano-Leaf/Vein Bionic Structure of TiO<sub>2</sub>/MoS<sub>2</sub> Composites for Photoelectric Sensors, *Nanoscale*, 2017, **9**, 18194–18201.
- 15 R. Dai, A. Zhang, Z. Pan, A. M. Al-Enizi, A. A. Elzatahry, L. Hu and G. Zheng, Epitaxial Growth of Lattice-Mismatched Core-Shell TiO<sub>2</sub>@MoS<sub>2</sub> for Enhanced Lithium-Ion Storage, *Small*, 2016, **12**, 2792–2799.
- 16 J. Liang, C. Wang, P. Zhao, Y. Wang, L. Ma, G. Zhu, Y. Hu, Z. Lu, Z. Xu, Y. Ma, T. Chen, Z. Tie, J. Liu and Z. Jin, Interface Engineering of Anchored Ultrathin TiO<sub>2</sub>/MoS<sub>2</sub> Heterolayers for Highly-Efficient Electrochemical Hydrogen Production, *ACS Appl. Mater. Interfaces*, 2018, **10**, 6084–6089.
- 17 Q. Xiang, J. Yu and M. Jaroniec, Synergetic Effect of MoS<sub>2</sub> and Graphene as Cocatalysts for Enhanced Photocatalytic H<sub>2</sub> Production Activity of TiO<sub>2</sub> Nanoparticles, *J. Am. Chem. Soc.*, 2012, **134**, 6575–6578.
- 18 L. Zheng, S. Han, H. Liu, P. Yu and X. Fang, Hierarchical MoS<sub>2</sub> Nanosheet@TiO<sub>2</sub> Nanotube Array Composites with Enhanced Photocatalytic and Photocurrent Performances, *Small*, 2016, **12**, 1527–1536.
- 19 B. Chen, Y. Meng, J. Sha, C. Zhong, W. Hu and N. Zhao, Preparation of MoS<sub>2</sub>/TiO<sub>2</sub> based Nanocomposites for Photocatalysis and Rechargeable Batteries: Progress, Challenges, and Perspective, *Nanoscale*, 2017, **10**, 34–68.
- 20 J. Zheng, X. Yan, Z. Lu, H. Qiu, G. Xu, X. Zhou, P. Wang, X. Pan, K. Liu and L. Jiao, High-Mobility Multilayered MoS<sub>2</sub>



- Flakes with Low Contact Resistance Grown by Chemical Vapor Deposition, *Adv. Mater.*, 2017, **29**, 1604540.
- 21 T.-Y. Chen, Y.-H. Chang, C.-L. Hsu, K.-H. Wei, C.-Y. Chiang and L.-J. Li, Comparative Study on MoS<sub>2</sub> and WS<sub>2</sub> for Electrocatalytic Water Splitting, *Int. J. Hydrogen Energy*, 2013, **38**, 12302–12309.
  - 22 Q. Pang, Y. Zhao, X. Bian, Y. Ju, X. Wang, Y. Wei, B. Liu, F. Du, C. Wang and G. Chen, Hybrid Graphene@MoS<sub>2</sub>@TiO<sub>2</sub> Microspheres for Use as a High Performance Negative Electrode Material for Lithium Ion Batteries, *J. Mater. Chem. A*, 2017, **5**, 3667–3674.
  - 23 Y. Liu, H. Niu, W. Gu, X. Cai, B. Mao, D. Li and W. Shi, In situ Construction of Hierarchical CdS/MoS<sub>2</sub> Microboxes for Enhanced Visible-Light Photocatalytic H<sub>2</sub> Production, *Chem. Eng. J.*, 2018, **339**, 117–124.
  - 24 L. Zhao, T. Dong, J. Du, H. Liu, H. Yuan, Y. Wang, J. Jia, H. Liu and W. Zhou, Synthesis of CdS/MoS<sub>2</sub> Nanooctahedrons Heterostructure with a Tight Interface for Enhanced Photocatalytic H<sub>2</sub> Evolution and Biomass Upgrading, *Sol. RRL*, 2021, **5**, 2000415.
  - 25 M. Yang, L. Wang, G. Hu, X. Chen, P. L. Gong, X. Cong, Y. Liu, Y. Yang, X. Li, X. Zhao and X. Liu, Optical Identification of Interlayer Coupling of Graphene/MoS<sub>2</sub> van der Waals Heterostructures, *Nano Res.*, 2021, **14**, 2241–2246.
  - 26 W. Zhou, K. Zhou, D. Hou, X. Liu, G. Li, Y. Sang, H. Liu, L. Li and S. Chen, Three-Dimensional Hierarchical Frameworks Based on MoS<sub>2</sub> Nanosheets Self-Assembled on Graphene Oxide for Efficient Electrocatalytic Hydrogen Evolution, *ACS Appl. Mater. Interfaces*, 2014, **6**, 21534–21540.
  - 27 X. Liu, Z. Xing, H. Zhang, W. Wang, Y. Zhang, Z. Li, X. Wu, X. Yu and W. Zhou, Fabrication of 3D Mesoporous Black TiO<sub>2</sub>/MoS<sub>2</sub>/TiO<sub>2</sub> Nanosheets for Visible-Light-Driven Photocatalysis, *ChemSusChem*, 2016, **9**, 1118–1124.
  - 28 W. Zhou, Z. Yin, Y. Du, X. Huang, Z. Zeng, Z. Fan, H. Liu, J. Wang and H. Zhang, Synthesis of Few-Layer MoS<sub>2</sub> Nanosheet-Coated TiO<sub>2</sub> Nanobelt Heterostructures for Enhanced Photocatalytic Activities, *Small*, 2013, **9**, 140–147.
  - 29 Y. Yuan, Z. Ye, H. Lu, B. Hu, Y. Li, D. Chen, J. Zhong, Z. Yu and Z. Zou, Constructing Anatase TiO<sub>2</sub> Nanosheets with Exposed (001) Facets/Layered MoS<sub>2</sub> Two-Dimensional Nanojunctions for Enhanced Solar Hydrogen Generation, *ACS Catal.*, 2015, **6**, 532–541.
  - 30 K. He, Q. Wen, C. Wang, B. Wang, S. Yu, C. Hao and K. Chen, A Facile Synthesis of Hierarchical Flower-Like TiO<sub>2</sub> Wrapped with MoS<sub>2</sub> Sheets Nanostructure for Enhanced Electrorheological Activity, *Chem. Eng. J.*, 2018, **349**, 416–427.
  - 31 J. Lin, L. Zhao, Y. Heo, L. Wang, F. Bijarbooneh, A. Mozer, A. Nattestad, Y. Yamauchi, S. Dou and J. Kim, Mesoporous Anatase Single Crystals for Efficient Co<sup>(2+/3+)</sup>-Based Dye-Sensitized Solar Cells, *Nano Energy*, 2015, **11**, 557–567.
  - 32 K. Chang and W. Chen, L-Cysteine-Assisted Synthesis of Layered MoS<sub>2</sub>/Graphene Composites with Excellent Electrochemical Performances for Lithium Ion Batteries, *ACS Nano*, 2011, **5**, 4720–4728.
  - 33 Q. Zhou, W. Li, M. Gao, H. Xu, Y. Guo, L. Sun, D. Zheng and J. Lin, A Truncated Octahedron Metal-Organic Framework Derived TiO<sub>2</sub>@C@MoS<sub>2</sub> Composite with Superior Lithium-Ion Storage Properties, *J. Power Sources*, 2022, **518**, 230746.
  - 34 J. Yang, L. Yu, B. Zheng, N. Li, J. Xi and X. Qiu, Carbon Microtube Textile with MoS<sub>2</sub> Nanosheets Grown on Both Outer and Inner Walls as Multifunctional Interlayer for Lithium–Sulfur Batteries, *Adv. Sci.*, 2020, **7**, 1903260.
  - 35 S. Wang, B. Guan, L. Yu and X. (David), Lou, Rational Design of Three-Layered TiO<sub>2</sub>@Carbon@MoS<sub>2</sub> Hierarchical Nanotubes for Enhanced Lithium Storage, *Adv. Mater.*, 2017, **29**, 1702724.
  - 36 J. Pei, H. Geng, E. H. Ang, L. Zhang, X. Cao, J. Zheng and H. Gu, Controlled Synthesis of Hollow C@TiO<sub>2</sub>@MoS<sub>2</sub> Hierarchical Nanospheres for High-Performance Lithium-Ion Batteries, *Nanoscale*, 2018, **10**, 17327–17334.
  - 37 B. Guo, K. Yu, H. Fu, Q. Hua, R. Qi, H. Li, H. Song, S. Guo and Z. Zhu, Firework-Shaped TiO<sub>2</sub> Microspheres Embedded with Few-Layer MoS<sub>2</sub> as an Anode Material for Excellent Performance Lithium-Ion Batteries, *J. Mater. Chem. A*, 2015, **3**, 6392–6401.
  - 38 S. V. P. Vattikuti and C. Byon, Synthesis and Characterization of Molybdenum Disulfide Nanoflowers and Nanosheets: Nanotribology, *J. Nanomater.*, 2015, **2015**, 1–11.
  - 39 X. Hu, H. Zhao, J. Tian, J. Gao, Y. Li and H. Cui, Synthesis of Few-Layer MoS<sub>2</sub> Nanosheets-Coated TiO<sub>2</sub> Nanosheets on Graphite Fibers for Enhanced Photocatalytic Properties, *Sol. Energy Mater. Sol. Cells*, 2017, **172**, 108–116.
  - 40 Q. Zhang, Y. Wang, X. Zhu, X. Liu and H. Li, 1T and 2H Mixed Phase MoS<sub>2</sub> Nanobelts Coupled with Ti<sup>3+</sup> Self-Doped TiO<sub>2</sub> Nanosheets for Enhanced Photocatalytic Degradation of RhB under Visible Light, *Appl. Surf. Sci.*, 2021, **556**, 149768.
  - 41 H. Yan, L. Liu, R. Wang, W. Zhu, X. Ren, L. Luo, X. Zhang, S. Luo, X. Ai and J. Wang, Binary Composite MoS<sub>2</sub>/TiO<sub>2</sub> Nanotube Arrays as a Recyclable and Efficient Photocatalyst for Solar Water Disinfection, *Chem. Eng. J.*, 2020, **401**, 126052.
  - 42 Z. Li, F. Cao, L. Wang, Z. Chen and X. Ji, A Novel Ternary MoS<sub>2</sub>/MoO<sub>3</sub>/TiO<sub>2</sub> Composite for Fast Photocatalytic Degradation of Rhodamine B under Visible-Light Irradiation, *New J. Chem.*, 2020, **44**, 537–542.
  - 43 D. Cao, Q. Wang, S. Zhu, X. Zhang, Y. Li, Y. Cui, Z. Xue and S. Gao, Hydrothermal Construction of Flower-Like MoS<sub>2</sub> on TiO<sub>2</sub> NTs for Highly Efficient Environmental Remediation and Photocatalytic Hydrogen Evolution, *Sep. Purif. Technol.*, 2021, **265**, 118463.
  - 44 M. Mohamed and N. Karunakaran, One-Step Solvothermal Synthesis of Carbon Doped TiO<sub>2</sub>–MoS<sub>2</sub> Heterostructure Composites with Improved Visible Light Catalytic Activity, *New J. Chem.*, 2016, **40**, 8123–8130.

